ACS APPLIED NANO MATERIALS

www.acsanm.org
Article

Optimizing Silver Nanowire Synthesis for In-Body Applications

Elif Sumeyye Cirit, Seda Aygul Akyuz, Ahmet Bilir, Sema Dumanli, Volkan Can, and Zeliha Cansu Canbek Ozdil*

Cite This: ACS Appl. Nano Mater. 2024, 7, 8130−8139

ABSTRACT: This work presents a parametric study for optimizing the synthesis of silver nanowires (AgNWs) using a polyol method for in-body applications. The effects of various parameters, including reaction time, reaction temperature, and type of metal halide employed during synthesis, on the properties of the AgNWs are systematically investigated. The kinetics of AgNW formation are analyzed by temporal UV−vis spectroscopy and TEM. To elaborate on the complexity of the metal halide employed during the production of silver nanowires, we have conducted various sets of experiments, revealing the role of the metal in classical polyol synthesis. We have demonstrated that even though the stoichiometric ratio of Ag^+/Cl^- is kept constant, the type of halide source is directly related to the formation of high-yield silver nanowires. The AgNW/P(AAm-*co*-AAc-*co*-PEGDA) hydrogel synthesized with as-produced AgNWs demonstrates suitable mechanical and electrical properties for in-body sensors, particularly for pH monitoring. Its electrical behavior exhibits frequency-dependent conductivity enhancements attributed to polarization mechanisms, but conductivity decreases with increasing pH due to ionization and structural changes within the hydrogel.

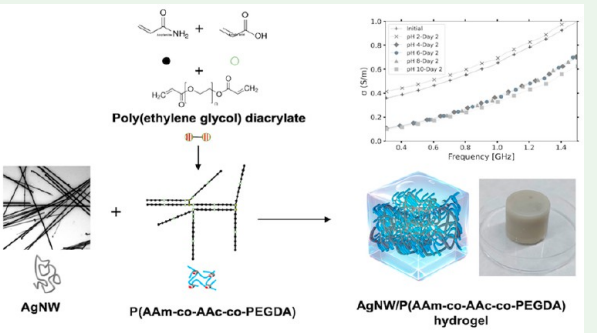

KEYWORDS: *silver nanowire, polyol synthesis, conductive hydrogel, in-body sensing, nanobiomaterial*

1. INTRODUCTION

The research in the field of implantable and wearable electronics has gained acceleration in parallel with the developments in new advanced materials and technologies.[1] These devices have numerous applications in the biomedical field since they offer unique properties such as adaptability, biocompatibility, foldability, bendability, stretchability, light weight, and comfortable utilization in comparison to rigid and tough electronics.[2]

With the recent advancements in nanotechnology, metallic nanoparticles with various morphologies are emerging as conductive elements since they can provide high stretchability under large deformation without failure compared with bulk rigid metals.[3] Metal nanowires with a high aspect ratio are highly popular as conductive elements due to the formation of a percolating network. Among various metals, silver nanowires have become the primary research focus. This is because they have a lower cost and are easier to produce than gold and platinum, and they offer higher electrical conductivity and resistance to oxidation than copper.[3,4] Furthermore, because of their natural antibacterial properties, biocompatibility, and corrosion resistance, silver nanowires are an excellent choice for in-body sensing applications. These attributes guarantee the long-term and reliable functioning of biomedical devices inside the human body. In particular, such systems are ideal candidates as conductive elements especially in wearable electronics since it is possible to create high-performance transparent thin conductive films with low sheet resistance or highly stretchable metal electrodes.[5−7] Beyond their conventional use, silver nanowires can be utilized as doping elements in the liquid form.

Several strategies have been developed in the last decades to produce high-yield monodisperse silver nanowires, which can be grouped under two main categories; hard template and soft template methods. In hard template production, nanoporous membranes, carbon nanotubes, and DNA molecules are used as hard templates.[8] The shape, size, and morphology of silver nanowires can be controlled by tuning the pore sizes of the templates. While the main advantage of using hard templates is offering uniform and well-defined morphologies by assisting the template, the drawbacks are the requirement for complex and damaging template removal processes, low yield, and the fact that they are not scalable for industrial applications.[9] That is why the researchers focused on soft templates such as

Received: February 2, 2024
Revised: March 8, 2024
Accepted: March 8, 2024
Published: April 1, 2024

Scheme 1. Schematic Representation of AgNW Formation Mechanism for As-Prepared AgNWs[a]

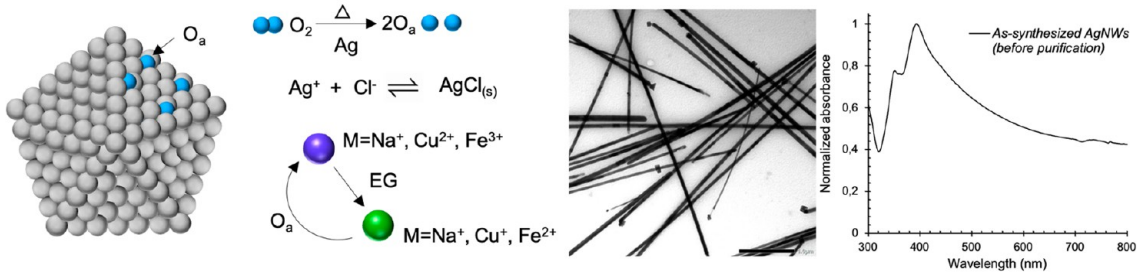

[a]Adapted from ref 25.

micelles, surfactants, and other polymers that are dissolvable in solvents to overcome these disadvantages of using hard templates, thus offering easy purification of nanowires from the solvents with improved efficiency and scalability.[9,10] In 2002, Xia's group proposed using polyvinylpyrrolidone (PVP) as a capping agent to produce large AgNWs (lengths of up to ~50 μm) with a high yield.[11,12] This has been the most successful strategy for the synthesis of AgNWs with high aspect ratios. This method is also called the polyol method since ethylene glycol (EG) is used both as a solvent and as a reductant in the synthesis whereas metal halide salt serves as a shape-directing agent.[13,14] The researchers have modified the polyol method by changing the reaction parameters, including the temperature,[15,16] the duration of the reaction,[17] the stirring rate,[18] the molecular weight of the capping agent,[19] the ratio of reactants,[20] the speed of material injection,[16] and the type of metal halide salt used to promote anisotropic growth[21,22] to tune the morphology of the resulting product. Each of these variables has a strong effect on the dimensions and characteristics of the resulting silver nanowires. Therefore, the polyol method became the most well-known and preferred synthesis route to produce AgNWs.[9,16,23−26]

Notwithstanding all of these efforts to create defined-size and structured anisotropic silver nanowires, the growth mechanism of such morphology is still under discussion. Even though it is well-known how to tune the aspect ratio of the final silver nanowires, understanding the effect of the reaction parameters on the size and yield of final nanowires is necessary to understand the path to anisotropic growth. Additionally, what is absolute is that to benefit from the enhanced properties of anisotropic silver nanostructures for any application, one should obtain a high yield of nanomaterials with a repeatable and reproducible process. Without an adequate protocol, the properties of materials change with each experiment. In the polyol reduction method, which is also known as a self-seeding process, it is assumed that the nucleation starts with the reduction of $AgNO_3$ which later on evolves into isotropic decahedron structure silver seeds. The anisotropic growth is achieved with the selective attachment of Ag ions on the (111) twin plane rather than the (100) plane on the decahedron structured seed due to strongly attached PVP on the (100) plane[16,27] as represented in Scheme 1.

In this study, we have focused on analyzing the effects of the reaction time, metal halide type, and reaction temperature to evaluate their impact on the development of anisotropy in silver nanowires by using the polyol method. The method has been chosen due to its long reaction kinetics and to provide substantial information to build a liaison between the small seeds and final nanoparticles. The significance of our work lies in the systematic approach employed for the optimization of the synthesis of AgNWs, which involved the utilization of a polyol. Particularly, the following analyzed conditions are selected with respect to the reference condition, mostly adapted from the literature where NaCl is used during production:

1. Reaction time (20 and 30 min)
2. Reaction temperature (110 °C, 130 °C, 150 °C, and 170 °C)
3. Three kinds of shape-mediating agents, NaCl, $CuCl_2$, and $FeCl_3$, are used without changing the stoichiometric ratio of Ag^+/Cl^-

In the second part of the study, we prepared a pH-responsive AgNW-based polyacrylamide hydrogel with as-synthesized nanowires and monitored the conductivity/permittivity change of the system. The obtained nanogel boasts high electrical conductivity attributed to its nanomaterial composition that can be used in in-body sensing applications. The core mechanism of the sensor hinges on its sensitivity to environmental pH changes, which, in turn, alters its electrical conductivity. The incorporation of AgNWs into a hydrogel matrix for in-body sensing applications enhances the versatility and practicality of the synthesized AgNWs creating a novel aspect for the use of the material as an implant sensor. Recent developments in implant sensors have revolutionized the healthcare system by monitoring various physical properties within the human body. In ref 28 a wireless implant sensor is envisaged where the electrical properties of the implant are altered with a physical parameter of interest to be sensed. This alteration, hence the physical parameter, can wirelessly be monitored from outside the human body through electromagnetic waves. An example can be given where the physical parameter of interest is pH. If a silver nanowire-doped hydrogel implant in the shape of a cylinder changes in size with the pH of its surroundings, the volume conductivity is going to change. If an electromagnetic wave is transmitted toward the implant and the reflected wave is collected with a receiver, the received signal has the signature of the implant. Hence the change in the volume conductivity of the implant is going to be visible in the reflected wave if the size of the implant and the wavelength of the electromagnetic wave are comparable. This dynamic response is critical for the detection of postoperative infections. The nanogel-based sensor operates without an internal power source. This approach not only promises a minimally invasive monitoring solution but also circumvents the limitations and risks associated with battery-powered implants, marking a significant advancement in postoperative care and infection management.

https://doi.org/10.1021/acsanm.4c00625
ACS Appl. Nano Mater. 2024, 7, 8130−8139

2. MATERIALS AND METHODS

2.1. Materials. Silver nitrate ($AgNO_3$), polyvinylpyrrolidone (PVP 40K), sodium chloride (NaCl), copper(II) chloride ($CuCl_2$), iron(III) chloride ($FeCl_3$), acrylic acid (AAc), acrylamide (AAm), polyethylene glycol diacrylate (PEGDA), and ammonium persulfate (APS) were obtained from Sigma-Aldrich and used without further purification except for ethylene glycol (EG, anhydrous, > 99%), which is purchased from Zag Chemicals. Before experiments, all glassware is cleaned with aqua regia and washed with distilled water. During the preparation of AgNW-based conductive ink, Milli-Q water with a resistivity value of 18.2 MΩ cm is used.

2.2. Methods. *2.2.1. Synthesis and Purification of AgNWs.* A 0.9 M PVP solution is prepared in 50 mL of EG. The solution is transferred to a round-bottom flask and heated to 170 °C for one h under continuous stirring. After 1 h, a defined amount of metal halide used as a shape mediating agent is added to the PVP solution and stirred for 10 min before adding the silver precursor for different synthesizes. Following that, 50 mL of 0.06 M $AgNO_3$/EG solution is added to the mixture via a syringe pump with an injection speed of 2.5 mL/min. After all $AgNO_3$ solutions were added, the mixture is stirred at 170 °C unless indicated otherwise for a different set of experiments. The final concentrations of the reagents used during production are summarized in Table 1.

Table 1. Final Concentrations of Chemical Reagents Used during the Synthesis of AgNWs

	[Metal halide]$_{final}$ (mM)			
[PVP]$_{final}$ (M)	[NaCl]	[$CuCl_2$]	[$FeCl_3$]	[$AgNO_3$]$_{final}$ (M)
0.045	0.150	0.075	0.050	0.030

During the kinetic measurements, 100 μL of the solution is taken from the mixture and diluted with EG to slow down the nanoparticle growth. The obtained nanoparticles are purified via centrifugation with the three-step protocol. First, the solution is centrifuged at 3000 rpm for 10 min, and the sediments are separated from the supernatant. In the second step, the sediment is redispersed in 15 mL of acetone and centrifuged again at 3000 rpm for 10 min. After the supernatant separation, 10 mL of ethanol is added to the sediment and centrifuged at 3000 rpm for 10 min one last time. Finally, the obtained silver nanowires are redispersed in 3 mL of ethanol.

2.2.2. Characterization of AgNWs. Multiple approaches are used to characterize the silver nanowires. UV−vis spectroscopy is used to examine the absorption properties of the material across a wide range of wavelengths. The UV−vis spectra are collected before the purification step. The HORIBA DUETTA Absorption and Fluorescence Spectrophotometer is used to collect the kinetic spectra in a 10 mm-Helma cell. Ezpec software is used to examine the data. A JEOL JEM 2100 Plus microscope equipped with a Gatan US4000 CCD camera running at 200 kV is used to conduct the TEM observations. The size distribution of isotropic nanoparticles is measured using the Malvern Zetasizer Nano Z instrument. The analyses are realized at 25 °C and measured in general-purpose mode; the autocorrelation function is used to derive the volume size distribution.

2.2.3. Synthesis of AgNW/P(AAm-co-AAc-co-PEGDA) Hydrogels. For the synthesis of pH-sensitive P(AAm-*co*-AAc-*co*-PEGDA) gel, the polymer concentration is set at 10% (w/v). Hydrogel preparation has been conducted as follows: 0.8 g of acrylamide monomer is dissolved in 8 mL of DIW in a 20 mL glass vial, and 0.2 g (190 μL) of acrylic acid is added to this mixture. Following that, 0.1966 g of PEGDA as cross-linker is added and dissolved. After the addition of 1 mL of%10 wt. AgNW aqueous solution, the reaction mixture is cooled down to +4 °C with the help of an ice−water bath under an inert Argon atmosphere for 15 min, and 0.016 g ammonium persulfate (APS) was added and dissolved in order to initiate the polymerization. The vial is then capped, and the polymerization reaction is carried out at room temperature of 25 °C.

2.2.4. Characterization of pH-Sensitive AgNW/P(AAm-co-AAc-co-PEGDA) Hydrogels. 2.2.4.1. Swelling Experiments. Swelling characteristics of the AgNW/P(AAm-co-AAc-co-PEGDA) hydrogel are analyzed by using the gravimetric method. The as-synthesized hydrogel samples are weighed and immersed into an excess amount of pH 2 buffer solution at room temperature. At 2 day intervals, the hydrogels are taken out of the buffer, blotted to remove surface water, and weighed. The same procedure is repeated for pH 4, 6, 8, and 10 buffer solutions. The equilibrium weight swelling ratio (m_{eq}) is calculated as

$$m_{eq} = \frac{m}{m_0}$$

where m and m_0 are the masses of the gels at equilibrium swelling and as-synthesized states, respectively.

2.2.4.2. Rheological Characterization. Rheological measurements are carried out with an Anton Paar rheometer, model MCR302e, equipped with Peltier technology, a temperature controller that allows additional plates with desired properties to be fixed on it, and a passive (no temperature control) cap on top. A 25 mm diameter bottom plate with sandblasted surface is mounted on the temperature controller, and measurements are taken at 25 °C. A 25 mm diameter plate with a sand-blasted surface is used as the upper measuring plate. Sandblasted plates are preferred to increase the adhesion of the sample with the plate surfaces and to prevent measurement errors that may occur due to the possible slipping of the sample from the surface, especially at high strain values in the nonlinear region. In addition, to prevent slipping of the sample, pressure is applied with a force of approximately 10 N to ensure that the contact between the samples and the plates is fully ensured.

The samples are subjected to frequency sweep tests. The frequency is selected as 10 rad/s. In the frequency sweep; frequency values are reduced logarithmically from 100 to 0.1 rad/s by taking a total of 19 data at 1% strain value selected from the linear viscoelastic region. The data collection time is determined by the device.

2.2.4.3. Conductivity Measurements. The conductivities of the samples (diameter of 27 mm and height of 22 mm) are measured using Speag's DAKS 3.5 dielectric measurement kit at room temperature. Surface water was carefully removed by a blotting before each measurement.

3. RESULTS AND DISCUSSION

3.1. Investigation of Reaction Parameters on the Final AgNWs. *3.1.1. Kinetics of AgNW Growth and Effect of Reaction Time.* Figure 1a shows the normalized UV−vis absorption spectra of solutions taken during kinetic measurements. At t = 1.5 min, a relatively symmetric plasmon resonance peak centered at ∼415 nm indicates the formation of spherical silver nanoparticles. The plasmon peak broadens and shows a red shift between 1.50 and 10 min. This indicates the elongation of nanoparticles into rod-shaped structures. Additionally, the transverse plasmon resonance peak of AgNWs at ∼380 nm and a shoulder at ∼350 nm start to appear at t = 10 min. After 10 min, the intensities of the peaks at ∼380 nm and ∼350 nm start to increase due to the further anisotropic growth toward AgNWs. Therefore, the peak at ∼415 nm is not visible after 15 min, indicating the disappearance of spherical shapes.

The size distribution analysis realized via DLS of nanoparticles belonging to the sample taken at the fifth minute of the reaction can be seen in Figure 1b. The average diameter is found to be 15 ± 6 nm. On the other hand, the average diameter of anisotropic nanoparticles at the bifurcation point, where the symmetry is broken, and at the later stages of growth, is calculated according to UV−vis spectra by using the mathematical relation developed by Azani and Hassanpour.[29] Figure 1c depicts the evaluation of the nanoparticle diameter

https://doi.org/10.1021/acsanm.4c00625
ACS Appl. Nano Mater. 2024, 7, 8130−8139

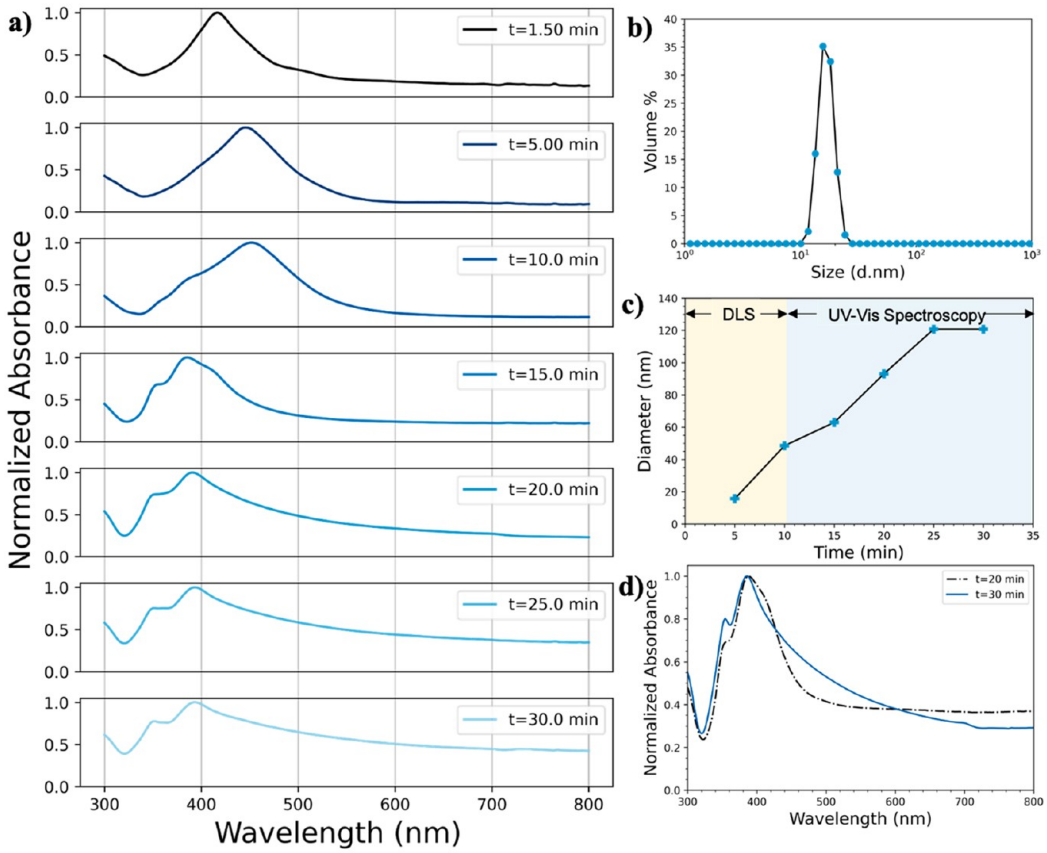

Figure 1. (a) Time evolution of the normalized absorption spectra for AgNWs synthesized at 170 °C with NaCl. (b) The volume-based size distribution data are obtained from DLS for 5 min. (c) The temporal change in the diameter of AgNWs. (d) A comparison between the extinction spectra of the reaction carried at 170 °C for a duration of 20 and 30 min.

throughout the growth of silver nanowires. As seen clearly, the enlargement of nanowires does not stop at 20 min; instead, they continue to grow until 25 min into the reaction. A stable plateau is observed between 25 and 30 min of reaction with a calculated diameter of 120.7 nm, indicating no further increase in diameter, thus signifying that the growth is complete.

In Figure 1d, a comparison between the normalized absorption spectra of the reactions conducted for 20 and 30 min is demonstrated. In the absorption spectrum of the reaction that lasted for 20 min, the peak around 415 nm can still be seen. This is because the intensities of the peaks around 350 and 390 nm, which indicate the anisotropic growth of the silver nanowires, have not increased sufficiently to impede the appearance of this peak. Furthermore, the spectrum of the reaction, which lasted for 30 min, has a broad transverse resonance peak at around 390 nm, indicating high morphological polydispersity. This outcome is consistent with the kinetic results showing that the reaction is not yet finished after 20 min.

AgNW growth is often explained via homogeneous nucleation, where initially small-sized decahedron seeds are formed, which are then grown into highly anisotropic nanorods and nanowires via the deposition of freshly formed silver atoms onto (111) planes and the Ostwald ripening process, where smaller isotropic nanoparticles before the bifurcation point are gradually consumed by the larger ones.[27,30] The TEM micrographs presented in Figure 2a–e corresponding to different stages of growth demonstrate the formation of discontinuous nanowires via the attachment of adjacent nanoparticles undergoing recrystallization and forming a linear aggregation rather than only growing in a particular direction from the starting point. This result is consistent with the literature[31,32] where discontinuous nanorods eventually merge with adjacent particles to form highly anisotropic nanowires within the constraints of the pipe-shaped soft templates. The process known as "oriented attachment" involves the direct merging of nanoparticles that have similar crystal structures, resulting in the formation of larger particles. In our case, coalescence between two separate nanoparticles having similar crystallographic orientations (111) can be seen in the TEM micrographs presented in Figure 2f–h.

The TEM images of AgNWs synthesized by varying the reaction time are presented in Figure 3. When the reaction lasts for 20 min, nanowires with interrupted structures can be observed with spherical-shaped nanoparticles along the PVP template (Figure 3a) rather than continuous wires. During the kinetic measurements, 100 μL of the solution was taken from the mixture and diluted with EG causing an interruption during the growth. This may yield cubic-shaped byproducts observed in the image. Additionally, it is a widely observed phenomenon that the formation of byproducts in various shapes such as cubes, spheres, and pyramids during polyol synthesis. This phenomenon is attributed to the etching process induced by an increase in the acidification of the reaction medium. Moreover, the byproducts remained in the sample due to the absence of any purification procedures

https://doi.org/10.1021/acsanm.4c00625
ACS Appl. Nano Mater. 2024, 7, 8130–8139

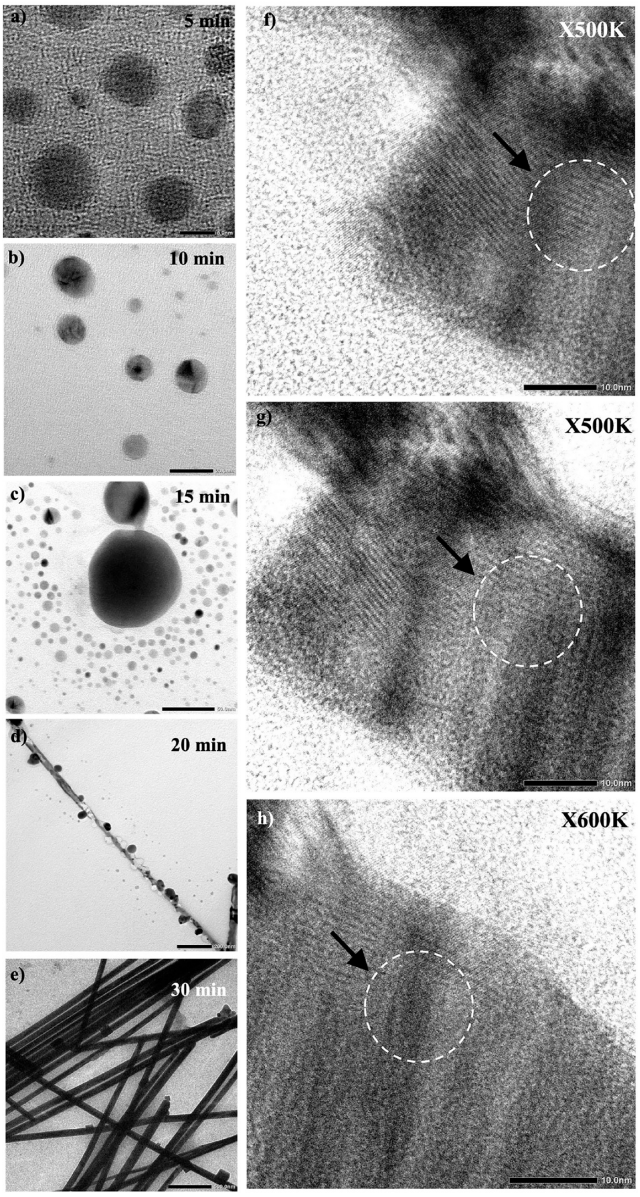

Figure 2. (a–e) TEM images of silver nanoparticles corresponding to kinetic measurements (scale bars are 5, 20, 50, 200, and 500 nm, respectively) and (f–h) HRTEM micrographs showing the coalescence of two particles with favorable crystallographic orientations.

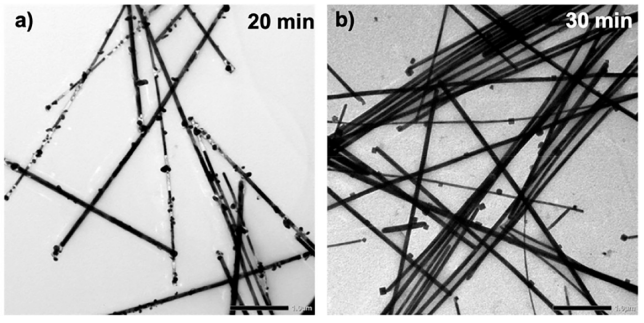

Figure 3. TEM images of AgNWs synthesized for (a) 20 min and (b) 30 min of reaction time.

applied to the kinetic measurement samples. In the case of a 30 min reaction, continuous nanowires are formed with cubic-shaped byproducts (Figure 3b). The average diameter and the length of the AgNWs is verified by using TEM and SEM images as 72 ± 8 nm and 9 ± 4 μm, respectively.

3.1.2. Effect of Reaction Temperature. To evaluate the effect of temperature, the AgNW synthesis is conducted at 110 °C, 130 °C, 150 °C, and 170 °C without changing other reaction parameters. Coskun et al. reported that when the reaction temperature is raised to 170 °C, the increased thermal energy enables the formation of multitwin particles, leading to a higher yield of Ag nanowires.[16] Elevating the reaction temperature further to 190 and 200 °C results in an increased number of multitwin particles formed early in the reaction, facilitated by the surplus thermal energy available for twinning. Consequently, initially formed Ag nanowires can reach lengths of up to 50 μm. However, a majority of nanowires exhibit low aspect ratios because the limited amount of Ag atoms relative to the numerous Ag nanowires prevents them from acquiring sufficient Ag atoms for further growth. We have seen a similar trend in our experimental studies. As a result of that, we have limited the reaction temperature to 170 °C.

Even though successful syntheses of silver nanowires have been reported below 130 °C,[33] suggesting that with adequate time, lower temperatures might yield desirable morphologies and recoveries, in this work we focused on a specific temperature range due to our objective of expediting the production of silver nanowires. Comparable observations are noted concerning the reaction duration.

The normalized absorbance spectra of these reactions can be seen in Figure 4a. In the spectrum of the reaction realized at 110 °C, two peaks at ∼415 and ∼510 nm are distinctly visible. As mentioned before, the peak at ∼415 nm represents the formation of isotropic silver nanoparticles, whereas the peak at ∼510 nm indicates the beginning of the anisotropy since it is the result of electron oscillation along the longitudinal axis of short nanorods. The longitudinal plasmon resonance peak shifts toward red to ∼510 nm as a result of the elongation of silver nanorods, as shown in the spectrum of the reaction at 130 °C. At 150 °C, there is only one peak at 422 nm on the spectrum, which is mainly due to the coalescence of the short nanorods to grow into longer aspect ratio nanowires, causing an overlap with the surface plasmon resonance (SPR) peak at ∼415 nm.

The optical characteristics of the metal nanoparticle solution demonstrate notable changes with increasing temperature, as depicted in Figure 4b. Particularly at elevated temperatures, there is a noticeable increase in the concentration of silver nanoparticles, which is evidenced by the change in the color and growing turbidity of the solution from light brown to grayish brown. Consistent with the findings of Coskun et al.,[16] our results indicate that the formation of high aspect ratio Ag nanowires is highly dependent upon a certain critical temperature threshold for given reaction times. At a lower temperature of 150 °C, the absence of the localized SPR (LSPR) in our observation points to the formation of isotropic silver nanoparticles rather than elongated nanowires. This further underscores the importance of high temperatures, not only for facilitating the synthesis of high aspect ratio Ag nanowires but also for enabling the conversion of ethylene glycol into glycolaldehyde, a crucial step for the reduction of Ag^+ ions to Ag atoms.

https://doi.org/10.1021/acsanm.4c00625
ACS Appl. Nano Mater. 2024, 7, 8130–8139

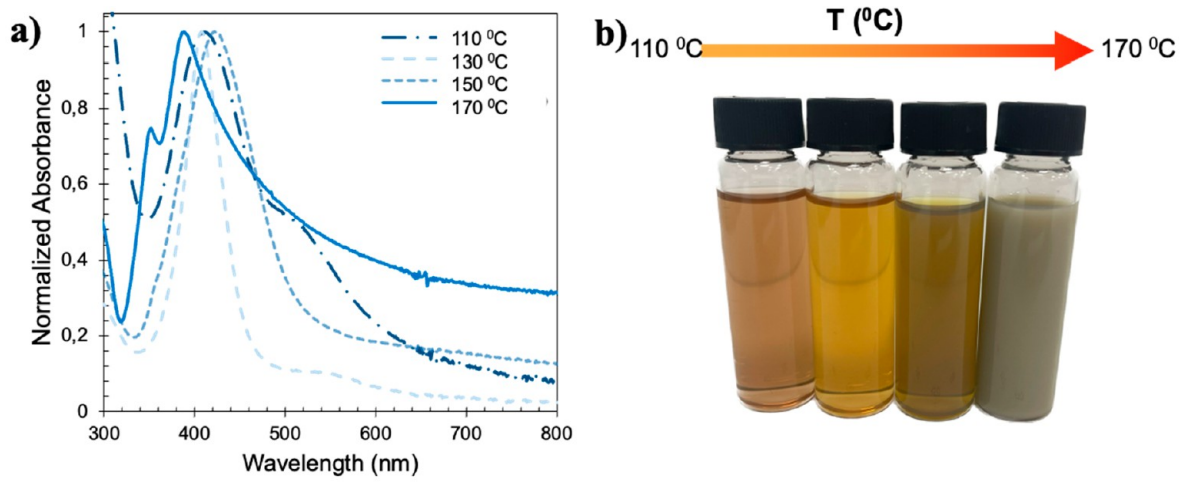

Figure 4. (a) The UV−vis absorption spectrum of AgNWs synthesized at varying temperatures from 110 to 170 °C (b) Photograph of aqueous solutions of AgNWs prepared with increasing temperatures (toward the right).

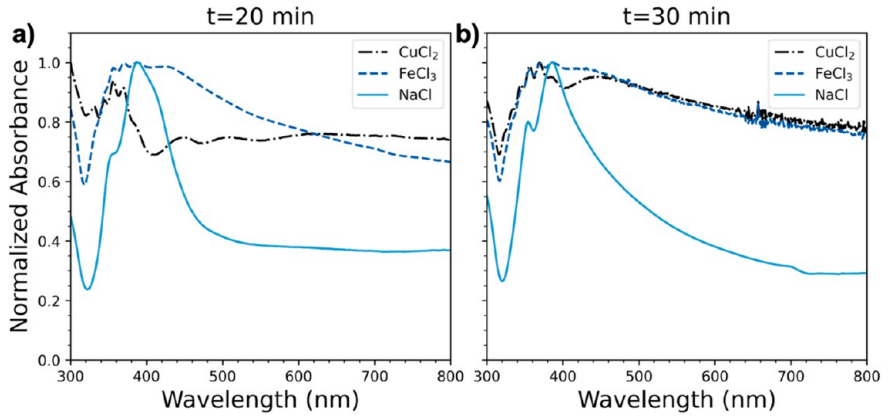

Figure 5. UV−vis Absorption spectrum of AgNWs prepared with NaCl, $CuCl_2$, and $FeCl_3$ for a duration of (a) 20 and (b) 30 min.

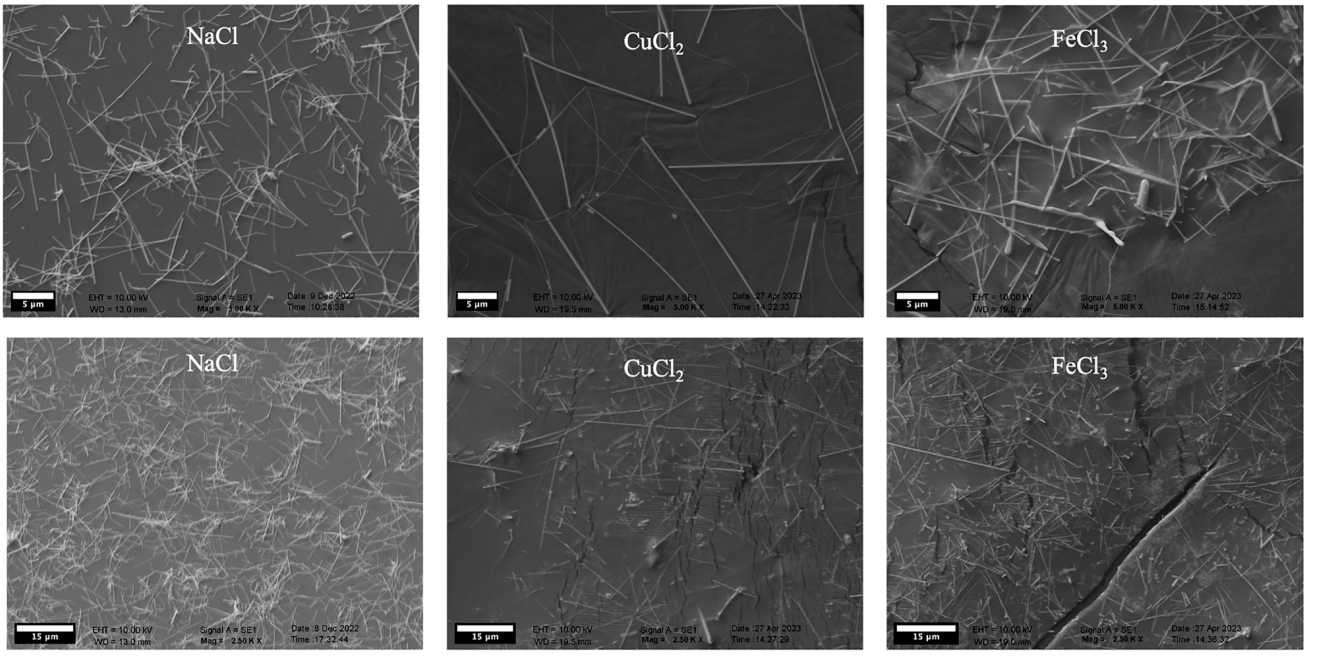

Figure 6. SEM images of AgNWs prepared with NaCl, $CuCl_2$, and $FeCl_3$ (t = 30 min).

https://doi.org/10.1021/acsanm.4c00625
ACS Appl. Nano Mater. 2024, 7, 8130−8139

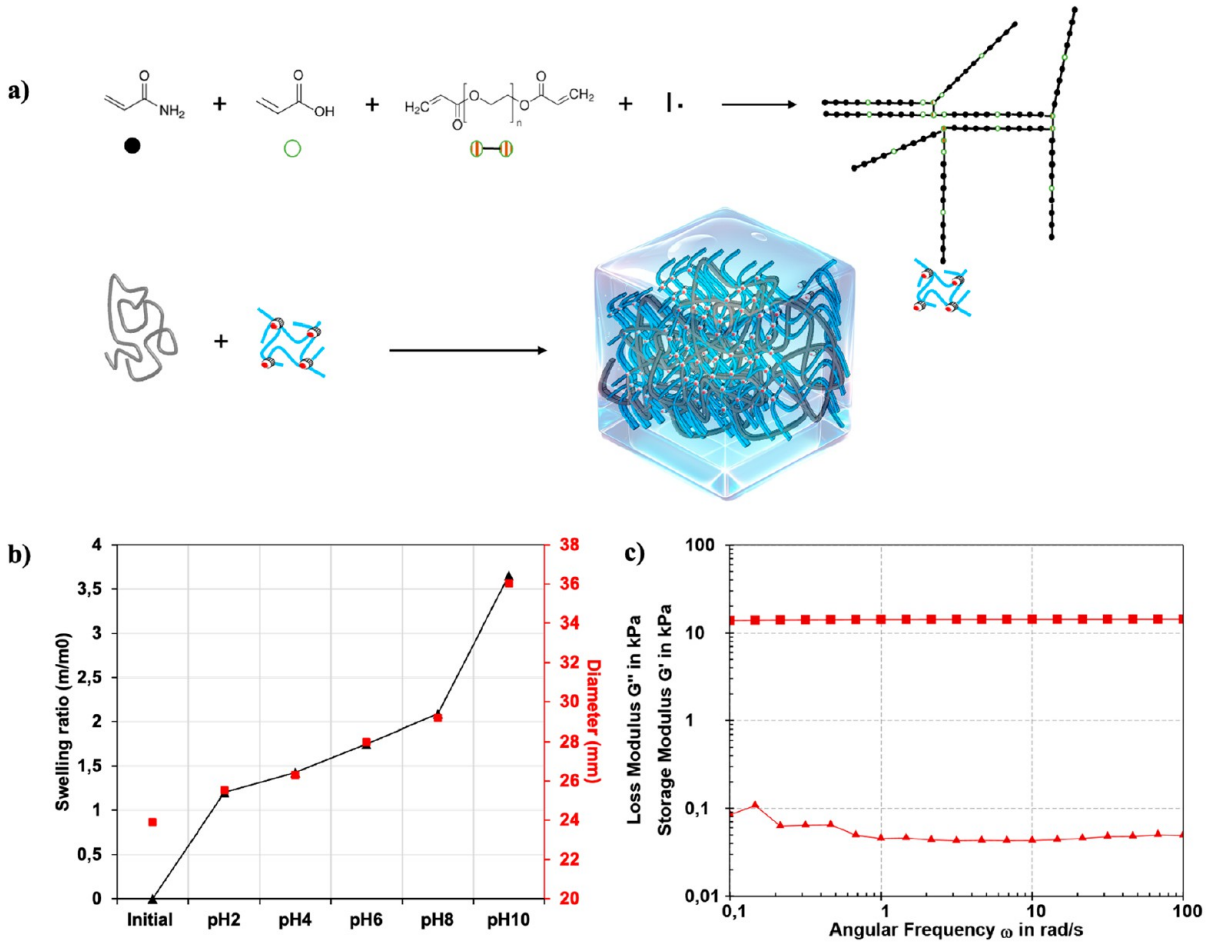

Figure 7. (a) Polymerization mechanism of AgNW/P(AAm-*co*-AAc-*co*-PEGDA) hydrogel. (b) Swelling behavior of the AgNW/P(AAm-*co*-AAc-*co*-PEGDA) hydrogel in response to pH over time. Storage modulus G' and loss modulus G'' versus (c) angular frequency sweep.

3.1.3. Effect of Metal Halide Counterion. Besides reaction time and temperature factors, the metal halide plays a significant role in determining the growth of silver nanowires. In general, NaCl is used during the synthesis to promote the slow deposition of Ag^+ ions via the formation of AgCl salt during the nucleation stage.[30,34] The formation of crystalline AgCl salt having low water solubility prevents supersaturation in the environment.[9,35] Without Cl^- in the environment, small-sized isotropic silver nanoparticles are formed due to rapid nucleation and growth of clusters at the same time in the reaction medium.

The effect of the mediating agent cation is another parameter that should be investigated. For the intended objective in question, we conducted several syntheses by using different metal halide salts, by fixing the stoichiometric ratio of Ag^+/Cl^- constant, in the polyol method while keeping the reaction temperature at 170 °C. Our primary objective in this work is to keep the Cl^- concentration uniform across the experiments rather than the metal halide concentration. This approach ensures that the influence of chloride ions on the shape and size evolution of Ag nanowires remains constant, allowing for a more accurate comparison of the effects of other variables on the synthesis process.

The UV−vis spectrum of the nanoparticles prepared by using NaCl, $CuCl_2$, and $FeCl_3$ is given below for two different reaction times (Figure 5a, b). In comparison to NaCl, the AgNWs prepared with $CuCl_2$, and $FeCl_3$ do not exhibit the distinct characteristic peaks of ∼350 and ∼390 nm corresponding to the AgNWs, but rather a large curve both for 20- and 30 min reaction times, indicating the formation of large nanowires and other byproducts. This is consistent with the Scanning electron microscopy (SEM) images of the corresponding samples presented in the Supporting Information in Figure 6.

The UV−visible spectroscopy data can be utilized to ascertain the yield of AgNW synthesis as suggested in the work of Azani and Hassanpour.[29] In the samples prepared using 0.075 mM $CuCl_2$ and 0.050 mM $FeCl_3$, two subtle peaks are observed at approximately 370 and 355 nm, corresponding to final AgNW concentrations of 0.041 and 0.043 g/L, respectively. These observations indicate yields of 37% and 34% for AgNWs. Conversely, in the sample synthesized with 0.150 mM NaCl, distinct surface plasmon resonance peaks are evident at approximately 395 and 355 nm, reflecting a concentration of 0.15761 g/L and yielding an 88% efficiency in AgNW production.

In comparison to $CuCl_2$ or $FeCl_3$, we have found NaCl to be a more effective shape-directing agent for the synthesis of higher-yield silver nanowires for the defined Cl^- concentration. One possible reason for this is related to the oxidative etching mechanism, which is a process that occurs during the synthesis of silver nanowires.[21,22,36] Oxidative etching is a surface-mediated reaction that involves the oxidation of silver ions by a strong oxidizing agent, which leads to the removal of silver

https://doi.org/10.1021/acsanm.4c00625
ACS Appl. Nano Mater. 2024, 7, 8130−8139

atoms from the surface of the nanowires. $CuCl_2$ and $FeCl_3$ have higher oxidizing power due to their high standard reduction potentials (0.16 and 0.77 V, respectively) compared to NaCl (−2.71 V), causing a strong etching of penta-twinned silver nanoparticles before growing.[37] In other words, at relatively low metal cation concentrations, in the presence of O_2, metal ions (Cu^{2+}, Fe^{3+}) can selectively etch other shapes, yielding penta-twinned seeds in the environment to grow into high-yield nanowires, whereas excess metal ions also cause the etching of 5-fold penta-twinned seeds before growing into nanowires. Our results are consistent with the literature,[21,22] indicating that there is an appropriate amount of Fe^{3+} and Cu^{2+} to generate high aspect ratio silver nanowires. The excess $CuCl_2$ and $FeCl_3$ concentrations yield shorter nanowires and large amounts of byproducts, such as spherical nanoparticles, cubes, and bipyramids. With our concentration range, we are below the stated amount of Cl^-.

3.2. AgNW/P(AAm-*co*-AAc-*co*-PEGDA) Hydrogels. Polymerization and cross-link reaction has been initiated via ammonium persulfate activation. Ammonium persulfate (APS) is a common redox initiator that is used for initiating the polymerization of acrylic-based water-soluble monomers. However, to activate APS at temperatures as low as room temperature, an additional activator such as N′,N′-tetramethyl ethylene diamine (TEMED) has to be used. Zerovalent transition metal nanoparticles such as iron, cobalt, and silver are also known to be used as persulfate activators in the following reactions[38] (eq 1):

$$Ag^0 + S_2O_8^{2-} \rightarrow Ag^+ + SO_4^{2-} + SO_4 \quad (1)$$

Silver nanowires that are utilized in this study have been observed to have such an activation effect on the APS radical initiator molecule. The proposed mechanism for radical generation is based on the activation of APS by the high surface energy of silver nanowires (Figure 7a).

The swelling behavior of the hydrogel in response to different pH environments over time is shown in Figure 7b. The mass swelling ratio of the hydrogel increases progressively starting from 1.2 and reaching 3.5 as the pH rises from 2 to 10. Also, the initial diameter has been changed from 21.9 to 35 mm by the change of pH from 2 to 10.

The rheological behavior of the AgNW/P(AAm-*co*-AAc-*co*-PEGDA) frequency sweep experiments is presented in Figure 7c. The linear viscoelastic region has been determined via amplitude sweep tests and according to the results, 1% of shear strain which is within the linear viscoelastic region has been selected for frequency sweep tests. During the frequency sweep tests, the storage modulus of the hydrogel does not show a significant change with increasing frequency from 0.1 to 100 rad/s (Table 2). During the whole frequency range G' has been measured higher than G'' and the trend has been recorded below 1 which indicates the viscoelastic solid-like behavior of the hydrogels. Additionally, the tan(δ) value which has been changed between 0.003 and 0.006 during the measurements, also implies that the elastic behavior dominates over the viscous behavior since this value is close to the ideal elastic behavior marker of 0.001. G', G'', and tan(δ) values have not significantly changed showing almost no dependence on the frequency in the experimental frequency range. This behavior indicates the domination of stable chemical cross-link points which hinders the energy dissipation during the deformation process in the studied concentration range. As a conclusion, the material is predominantly elastic, with its behavior only slightly influenced by frequency changes. This consistency in rheological response at different frequencies is beneficial for in-body applications where the material needs to withstand various mechanical stresses without permanent deformation.

Table 2. Angular Frequency Scan Results

	AgNW/P(AAm-co-AAc-co-PEGDA) hydrogels		
Angular frequency (rad/s)	G' (kPa)	G'' (kPa)	tan δ
0.1	13.80	0.05	0.003
1.0	14.12	0.04	0.003
10.0	14.19	0.05	0.003
100.0	14.25	0.08	0.006

Figure 8a and b shows the frequency-dependent alternating current (AC) conductivity of the AgNW/P(AAm-co-AAc-co-PEGDA) hydrogel, within the range of 300 MHz-6 GHz at different pH values to optimize the sensor's wireless communication performance by selecting the most suitable frequency range. Measurements of AC conductivity across various frequencies are employed to assess the efficacy of the hydrogel over a spectrum of AC frequencies. This evaluation is crucial for implantable electronic devices that function at diverse frequencies. The results show that at low-frequency values, the initial conductivity of the hydrogel is around 0.4 S m^{-1} and it increases to 7.5 S m^{-1} with the increase in frequency. As the pH increases from 2 to 10 the conductivity decreases drastically. The reason is that at higher pH levels, the acidic groups within the polymer network become ionized, causing an increase in the negative charge density within the hydrogel. This increased negative charge potentially causes a reduction in the overall ionic mobility and thus the conductivity. Additionally, during swelling, a higher water content may lead to a larger distance between cross-linking points and silver nanowires. This increased distance may reduce the mobility of ions if the network becomes too loose, thereby decreasing the conductivity.

As the hydrogel's electrical properties are sensitive to the pH of the environment, it is possible to use AgNW/P(AAm-co-AAc-co-PEGDA) hydrogel for the detection of postoperative infections as the next-generation wireless implant sensors.

4. CONCLUSION

In conclusion, this study provides insights into the optimization of the synthesis of AgNWs for in-body applications using a polyol method. Through a parametric study, the influence of reaction time, reaction temperature, and the type of metal halide employed during the synthesis on the properties of the resulting AgNWs have been demonstrated. The findings revealed that all of these parameters play a crucial role in determining the yield and aspect ratio of the AgNWs. When the reaction temperature is set at 170 °C and NaCl is used as a halide source, the growth of AgNWs completes in around 30 min, and high-yield AgNWs are obtained.

The AgNW/P(AAm-co-AAc-co-PEGDA) hydrogel prepared using the optimized synthesis conditions demonstrates the desired mechanical and electrical properties to be used as an integral component for in-body sensors for monitoring physical parameters within the human body, such as pH levels. The observed electrical behavior of the AgNW/P(AAm-co-AAc-co-PEGDA) hydrogel demonstrates a notable frequency-

https://doi.org/10.1021/acsanm.4c00625
ACS Appl. Nano Mater. 2024, 7, 8130−8139

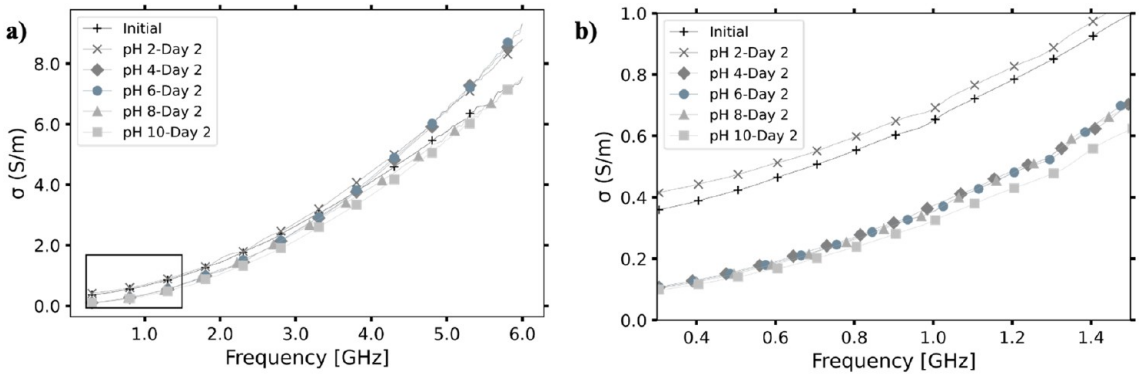

Figure 8. AC conductivity of AgNW/P(AAm-co-AAc-co-PEGDA) hydrogel as a function of frequency (a) within the frequency range of 300 MHz-6 GHz, (b) zoom in the frequency range: 0.2 GHz−1.5 GHz.

dependent increase in conductivity, which can be attributed to the various polarization mechanisms within the hydrogel matrix. At lower frequencies, the mobility of charge carriers is limited and polarization effects are less pronounced, resulting in lower conductivity. As the frequency of the applied electric field increases, polarization contributions, such as ionic and dipolar reorientations, become more significant, allowing the charge carriers to respond more rapidly, thereby enhancing the material's conductivity. Additionally, the decrease in conductivity with increasing pH from 2 to 10 suggests alterations in the hydrogel's ionic environment and the state of the silver nanowires. With the increase of the pH from 2 to 10, there is a significant reduction in conductivity. This is primarily because the acidic components of the polymer matrix tend to ionize more at elevated pH levels, leading to a surge in the negative charge density throughout the hydrogel structure. Such an escalation in the negative charge can impede the general movement of ions, thereby diminishing the conductivity. Furthermore, as the hydrogel swells, the incorporation of more water can expand the gap between the polymer's cross-links and the embedded silver nanowires, potentially inhibiting ion transport if the structural network becomes overly expanded, resulting in decreased conductivity.

AUTHOR INFORMATION

Corresponding Author

Zeliha Cansu Canbek Ozdil − *Department of Materials Science and Nanotechnology Engineering, Yeditepe University, Istanbul 34755, Turkey;* orcid.org/0000-0001-9420-567X; Email: cansu.canbek@yeditepe.edu.tr

Authors

Elif Sumeyye Cirit − *Department of Materials Science and Nanotechnology Engineering, Yeditepe University, Istanbul 34755, Turkey;* orcid.org/0009-0002-2137-8929

Seda Aygul Akyuz − *Department of Materials Science and Nanotechnology Engineering, Yeditepe University, Istanbul 34755, Turkey;* orcid.org/0009-0003-6464-3347

Ahmet Bilir − *Department of Electrical and Electronics Engineering, Bogazici University, Istanbul 34470, Turkey;* orcid.org/0000-0001-8315-8329

Sema Dumanli − *Department of Electrical and Electronics Engineering, Bogazici University, Istanbul 34470, Turkey;* orcid.org/0000-0002-5787-9429

Volkan Can − *Department of Genetics and Bioengineering and Automotive Technology Program, Yeditepe University, Istanbul 34755, Turkey;* orcid.org/0000-0001-8347-6335

Complete contact information is available at: https://pubs.acs.org/10.1021/acsanm.4c00625

Notes

The authors declare no competing financial interest.

ACKNOWLEDGMENTS

Financial support for this study was provided in part by the Turkish Scientific and Technical Research Council (TUBITAK) under contract number 22AG016, 23AG002 and Yeditepe University YAP Funding under grant number YAP-AAP-FEB-22033. The authors thank Anton Paar and HORIBA for their technical assistance.

REFERENCES

(1) Wang, S. A Comprehensive Review of Wearable Applications and Material Construction. *Open J. Appl. Sci.* **2020**, *10*, 364−408.

(2) Hassan, M.; Abbas, G.; Li, N.; Afzal, A.; Haider, Z.; Ahmed, S.; Xu, X.; Pan, C.; Peng, Z. Significance of Flexible Substrates for Wearable and Implantable Devices: Recent Advances and Perspectives. *Adv. Mater. Technol.* **2022**, *7* (3), 2100773.

(3) Park, J.; Hwang, J. C.; Kim, G. G.; Park, J.-U. Flexible Electronics Based on One-Dimensional and Two-Dimensional Hybrid Nanomaterials. *InfoMat* **2020**, *2* (1), 33−56.

(4) Han, S.; Hong, S.; Yeo, J.; Kim, D.; Kang, B.; Yang, M.-Y.; Ko, S. H. Nanorecycling: Monolithic Integration of Copper and Copper Oxide Nanowire Network Electrode through Selective Reversible Photothermochemical Reduction. *Adv. Mater.* **2015**, *27* (41), 6397−6403.

(5) Hu, M.; Gao, J.; Dong, Y.; Li, K.; Shan, G.; Yang, S.; Li, R. K.-Y. Flexible Transparent PES/Silver Nanowires/PET Sandwich-Structured Film for High-Efficiency Electromagnetic Interference Shielding. *Langmuir* **2012**, *28* (18), 7101−7106.

(6) Lee, P.; Lee, J.; Lee, H.; Yeo, J.; Hong, S.; Nam, K. H.; Lee, D.; Lee, S. S.; Ko, S. H. Highly Stretchable and Highly Conductive Metal Electrode by Very Long Metal Nanowire Percolation Network. *Adv. Mater.* **2012**, *24* (25), 3326−3332.

(7) Chen, J.-J.; Liu, S.-L.; Wu, H.-B.; Sowade, E.; Baumann, R. R.; Wang, Y.; Gu, F.-Q.; Liu, C.-R.-L.; Feng, Z.-S. Structural Regulation of Silver Nanowires and Their Application in Flexible Electronic Thin Films. *Mater. Des.* **2018**, *154*, 266−274.

(8) Kumar, A.; Shaikh, M. O.; Chuang, C.-H. Silver Nanowire Synthesis and Strategies for Fabricating Transparent Conducting Electrodes. *Nanomaterials* **2021**, *11* (3), 693.

(9) Zhang, P.; Wyman, I.; Hu, J.; Lin, S.; Zhong, Z.; Tu, Y.; Huang, Z.; Wei, Y. Silver Nanowires: Synthesis Technologies, Growth

Mechanism and Multifunctional Applications. *Mater. Sci. Eng., B* **2017**, *223*, 1−23.
(10) Zhang, P.; Lin, S.; Hu, J. Synthesis and Characterization of Size-Controlled Silver Nanowires. *Phys. Sci. Rev.***2018**, *3* (11), DOI: 10.1515/psr-2017-0084.
(11) Fievet, F.; Lagier, J. P.; Blin, B.; Beaudoin, B.; Figlarz, M. Homogeneous and Heterogeneous Nucleations in the Polyol Process for the Preparation of Micron and Submicron Size Metal Particles. *Solid State Ion.* **1989**, *32*−*33*, 198−205.
(12) Sun, Y.; Xia, Y. Large-Scale Synthesis of Uniform Silver Nanowires Through a Soft, Self-Seeding, Polyol Process. *Adv. Mater.* **2002**, *14* (11), 833−837.
(13) Fahad, S.; Yu, H.; Wang, L.; Zain-ul-Abdin; Haroon, M.; Ullah, R. S.; Nazir, A.; Naveed, K.-R.; Elshaarani, T.; Khan, A. Recent Progress in the Synthesis of Silver Nanowires and Their Role as Conducting Materials. *J. Mater. Sci.* **2019**, *54* (2), 997−1035.
(14) Skrabalak, S. E.; Wiley, B. J.; Kim, M.; Formo, E. V.; Xia, Y. On the Polyol Synthesis of Silver Nanostructures: Glycolaldehyde as a Reducing Agent. *Nano Lett.* **2008**, *8* (7), 2077−2081.
(15) Bergin, S. M.; Chen, Y.-H.; Rathmell, A. R.; Charbonneau, P.; Li, Z.-Y.; Wiley, B. J. The Effect of Nanowire Length and Diameter on the Properties of Transparent, Conducting Nanowire Films. *Nanoscale* **2012**, *4* (6), 1996−2004.
(16) Coskun, S.; Aksoy, B.; Unalan, H. E. Polyol Synthesis of Silver Nanowires: An Extensive Parametric Study. *Cryst. Growth Des.* **2011**, *11* (11), 4963−4969.
(17) Hu, M.; Gao, J.; Dong, Y.; Yang, S.; Li, R. K. Y. Rapid Controllable High-Concentration Synthesis and Mutual Attachment of Silver Nanowires. *RSC Adv.* **2012**, *2* (5), 2055−2060.
(18) Patil, S.; Kate, P. R.; Deshpande, J. B.; Kulkarni, A. A. Quantitative Understanding of Nucleation and Growth Kinetics of Silver Nanowires. *Chem. Eng. J.* **2021**, *414*, 128711.
(19) Zhu, J.-J.; Kan, C.-X.; Wan, J.-G.; Han, M.; Wang, G.-H. High-Yield Synthesis of Uniform Ag Nanowires with High Aspect Ratios by Introducing the Long-Chain PVP in an Improved Polyol Process. *J. Nanomater.* **2011**, *2011*, 982547.
(20) Fahad, S.; Yu, H.; Wang, L.; Nazir, A.; Ullah, R. S.; Naveed, K.-R.; Elshaarani, T.; Amin, B. U.; Khan, A.; Mehmood, S. Synthesis of Silver Nanowires with Controlled Diameter and Their Conductive Thin Films. *J. Mater. Sci. Mater. Electron.* **2019**, *30* (14), 12876−12887.
(21) Ma, J.; Zhan, M. Rapid Production of Silver Nanowires Based on High Concentration of AgNO3 Precursor and Use of FeCl3 as Reaction Promoter. *RSC Adv.* **2014**, *4* (40), 21060−21071.
(22) Johan, M. R.; Aznan, N. A. K.; Yee, S. T.; Ho, I. H.; Ooi, S. W.; Darman Singho, N.; Aplop, F. Synthesis and Growth Mechanism of Silver Nanowires through Different Mediated Agents (CuCl2 and NaCl) Polyol Process. *J. Nanomater.* **2014**, *2014*, 105454.
(23) Wiley, B.; Sun, Y.; Xia, Y. Polyol Synthesis of Silver Nanostructures: Control of Product Morphology with Fe(II) or Fe(III) Species. *Langmuir* **2005**, *21* (18), 8077−8080.
(24) Sun, Y.; Mayers, B.; Herricks, T.; Xia, Y. Polyol Synthesis of Uniform Silver Nanowires: A Plausible Growth Mechanism and the Supporting Evidence. *Nano Lett.* **2003**, *3* (7), 955−960.
(25) Korte, K. E.; Skrabalak, S. E.; Xia, Y. Rapid Synthesis of Silver Nanowires through a CuCl- or CuCl2-Mediated Polyol Process. *J. Mater. Chem.* **2008**, *18* (4), 437−441.
(26) Zhang, P.; Wei, Y.; Ou, M.; Huang, Z.; Lin, S.; Tu, Y.; Hu, J. Behind the Role of Bromide Ions in the Synthesis of Ultrathin Silver Nanowires. *Mater. Lett.* **2018**, *213*, 23−26.
(27) Roosen, A. R.; Carter, W. C. Simulations of Microstructural Evolution: Anisotropic Growth and Coarsening. *Phys. Stat. Mech. Its Appl.* **1998**, *261* (1), 232−247.
(28) Dumanli Oktar, S. *A System and Method Which Provides Wireless Communication between Bio-Nano Elements and Macro/Micro Devices*. WO2021126135A1.
(29) Azani, M.-R.; Hassanpour, A. Synthesis of Silver Nanowires with Controllable Diameter and Simple Tool to Evaluate Their Diameter, Concentration and Yield. *ChemistrySelect* **2019**, *4* (9), 2716−2720.
(30) Cao, L.; Huang, Q.; Cui, J.; Lin, H.; Li, W.; Lin, Z.; Zhang, P. Rapid and Facile Synthesis of High-Performance Silver Nanowires by a Halide-Mediated, Modified Polyol Method for Transparent Conductive Films. *Nanomaterials* **2020**, *10* (6), 1139.
(31) Lin, L.; Wang, W.; Huang, J.; Li, Q.; Sun, D.; Yang, X.; Wang, H.; He, N.; Wang, Y. Nature Factory of Silver Nanowires: Plant-Mediated Synthesis Using Broth of Cassia Fistula Leaf. *Chem. Eng. J.* **2010**, *162* (2), 852−858.
(32) Murph, S. E. H.; Murphy, C. J.; Leach, A.; Gall, K. A Possible Oriented Attachment Growth Mechanism for Silver Nanowire Formation. *Cryst. Growth Des.* **2015**, *15* (4), 1968−1974.
(33) Shi, Y.; Fang, J. Large-Scale Synthesis of High-Purity Silver Nanowires with Reduced Diameters by the Polyethylene Glycol-Assisted Polyol Method. *J. Phys. Chem. C* **2022**, *126* (46), 19866−19871.
(34) Chen, S.; Carey, J. L. I.; Whitcomb, D. R.; Bühlmann, P.; Penn, R. L. Elucidating the Role of AgCl in the Nucleation and Growth of Silver Nanoparticles in Ethylene Glycol. *Cryst. Growth Des.* **2018**, *18* (1), 324−330.
(35) Hemmati, S.; Harris, M. T.; Barkey, D. P. Polyol Silver Nanowire Synthesis and the Outlook for a Green Process. *J. Nanomater.* **2020**, *2020*, 9341983.
(36) Zheng, Y.; Zeng, J.; Ruditskiy, A.; Liu, M.; Xia, Y. Oxidative Etching and Its Role in Manipulating the Nucleation and Growth of Noble-Metal Nanocrystals. *Chem. Mater.* **2014**, *26* (1), 22−33.
(37) Petrucci, R. H.; Herring, F. G.; Madura, J. D.; Bissonnette, C. *General Chemistry Principles and Modern Applications*, 10th ed.; Learning Solutions: New York, 2011.
(38) Hejazi, S. A.; Zaheer, Z.; Kosa, S. A. Silver-Osmium Core-Shell Nanoparticles: Synthesis and Heterogeneous Persulfate Activator. *Mater. Chem. Phys.* **2023**, *305*, 127927.

https://doi.org/10.1021/acsanm.4c00625
ACS Appl. Nano Mater. 2024, 7, 8130−8139